As/Sb *threo*-monomethyltartrate(4-) and arsenic(III) *erythro*-monomethyltartrate systems are not reported here.

Conclusions

These studies are the first to demonstrate conclusively the presence of binuclear species as the principal constituents of aqueous solutions of antimony(III) and arsenic(III) tartrate(4-).[40] The (±)-dimethyltartrate(4-) and *threo*-monomethyltartrate(4-) complexes have been prepared and have also been shown to be dimeric. Evidence for binuclear structures includes (1) the observation of ^{13}C NMR spectra of mixed As/Sb complexes, (2) observed long-range $^{13}C-^{1}H$ coupling involving carbon and hydrogen atoms on separate ligands in the 2:2 species, and (3) the detection of both proximal-methyl and distal-methyl isomers of the monomethyltartrate(4-)-bridged complexes. The predicted[14] stability ordering *dd* (*ll*) > *dl* has been confirmed for these binuclear complexes. The chemical-shift changes accompanying formation of the mixed As/Sb complexes provide additional evidence that bond-angle changes are involved in steric ^{13}C NMR γ effects.[31] The long-range $^{13}C-^{1}H$ couplings observed for the tartrate(4-) complexes are probably due to multiple coupling pathways as a result of the polynuclear/polydentate ligand system.

Solid 1:1 complexes of arsenic(III) with *ms*-dimethyltartrate(4-) and *erythro*-monomethyltartrate(4-) have been prepared as the sodium salts. ^{13}C NMR spectra indicate that a principal (but not the only) species in aqueous solutions of the *ms*-dimethyltartrate salt is the binuclear β-$\Delta\Delta$(*ms*-*ms*), β-$\Lambda\Lambda$(*ms*-*ms*) pair of enantiomers. That these isomers have one of the two ionized hydroxyl oxygen atoms in each ligand in an axial coordination to the trigonal-bipyramidal arsenic atom may help stabilize these species. Arsenic(III) with its d^{10} electron configuration should prefer axial coordination by good π donors.[41] Some complexation of *ms*-tartrate with arsenic(III) has also been demonstrated. Complexation of antimony(III) with meso or erythro ligands, on the other hand, apparently takes place much less readily.

Extremely slow metal ion exchange kinetics have been observed in the formation of the mixed As/Sb (±)-dimethyltartrate(4-) complex and investigations are in progress.

Acknowledgments. This work was supported by the National Science Foundation, which supplied matching funds for the purchase of the Fourier transform system (Grant NPS75-06111), the University of New Mexico Research Allocations Committee, and the donors of the Petroleum Research Fund, administered by the American Chemical Society. The authors thank Dr. Ronald Light for his help with the collection of the ^{13}C NMR data.

(40) Potassium antimony(III) tartrate(4-) ("tartar emetic") exhibits an aqueous solution ^{13}C NMR spectrum similar to that of the sodium salt except for a small downfield shift of the two resonances (δ 183.71, 78.84 ppm). Sodium salts were used in these studies owing to their large solubilities. The chemical-shift differences between the potassium and sodium salts may be due to a small difference in the solution pH.[36]

(41) Rossi, A. R.; Hoffman, R. *Inorg. Chem.* **1975**, *14*, 365.

Soft X-ray Absorption Spectroscopy. Electronic and Morphological Structure of Poly(vinylidene fluoride)

R. S. Williams,[1a] D. Denley,[1a] D. A. Shirley,*[1a] and J. Stöhr[1b]

Contribution from the Materials and Molecular Research Division, Lawrence Berkeley Laboratory, and Department of Chemistry, University of California, Berkeley, California 94720, and the Stanford Synchrotron Radiation Laboratory, Stanford, California 94305.
Received July 12, 1979

Abstract: X-ray absorption studies were carried out for the first time on a polymeric thin film in the energy range 250–1000 eV, thereby providing access to the K edges of light elements. The carbon and fluorine K edges were studied in poly(vinylidene fluoride). Sharp peaks were observed at both edges, and extended fine structure (EXAFS) was found at higher energies. The carbon K edge showed compound structure, with a chemical shift of 3.9 eV between the C(1s) absorption energies in CH_2 and CF_2 groups. This type of shift is similar to, but not identical with, ESCA shifts. Fourier transformation of EXAFS structure above the F K edge yielded a C–F bond distance of 1.38 ± 0.02 Å and a second peak at 2.45 ± 0.08 Å, which is comprised of contributions from several neighbor shells, providing evidence of structural order. This method is concluded to be useful in studying polymeric electronic structure and molecular conformation.

I. Introduction

The increasing use of specialty polymers in the photographic and electronic industries has stimulated recent interest in their electronic properties.[2a] Among the most common experimental techniques employed to study polymer valence and conduction bands are X-ray and ultraviolet photoemission (XPS and UPS) and ultraviolet absorption (UVA) spectroscopies. These techniques yield complementary data, by probing both the occupied and vacant electronic states of a material for comparison with theoretical models. In addition to valence-band studies, XPS provides chemical-state information about each atomic species in a compound via chemical shifts in core-level binding energies.

To explore the electronic structure of polymers most effectively, both multitechnique analysis and theoretical understanding of the material studied are required. This paper presents the first utilization of soft X-ray absorption (SXAS) spectroscopy to study a thin-film polymer; the particular material studied was an ca. 5000 Å thick sample of poly(vinylidene fluoride) (PVF_2), an industrially important polymer[2b] (chemical formula $(CH_2CF_2)_n$). The results underscore several weaknesses of the above-mentioned spectroscopic techniques as applied to the study of polymers, and show that information obtained from SXAS data on the electronic and morphological properties of PVF_2 is indeed complementary to that obtained from electron spectroscopies, UVA, and even X-ray diffraction studies.

Section II presents a general discussion of several spectroscopic techniques which can elucidate polymer electronic structure. The

(1) (a) University of California, Berkeley; (b) Stanford Synchrotron Radiation Laboratory.

(2) (a) C. B. Duke, *J. Vac. Sci. Technol.*, **15**, 157 (1978); (b) A. L. Robinson, *Science*, **200**, 1371 (1978).

0002-7863/80/1502-5717$01.00/0 © 1980 American Chemical Society

types of information gained from each method, as well as their limitations, are contrasted with those of SXAS spectroscopy. In section III, the details of the thin-film sample preparation and the collection of the SXAS spectra are described. The spectra obtained in this investigation contain two distinct types of information, on electronic and morphological structure. Each is covered in a separate subsection (IVA and IVB). The absorption onset at the carbon K edge in PVF_2 is discussed in section IVA, with special emphasis on reference states for electronic properties, transitions to bound states below the ionization potential, and chemical-shift information. The fluorine K-edge spectrum is analyzed for its extended X-ray absorption fine structure (EXAFS) in section IVB, which yields an accurate determination of the F–C distance in PVF_2 as well as other structural information. Finally, section V concludes with several observations regarding the utility of SXAS spectroscopy as applied to polymer chemistry and a summary of the data gathered for PVF_2.

II. SXAS as a Polymer Electronic Structure Method

To be a viable technique for the study of any material, SXAS must provide clear advantages over the techniques listed in the Introduction and/or yield complementary data; in principle, SXAS fulfills both of these conditions. The most troublesome difficulty with photoemission experiments on insulating materials is sample charging caused by the ejected photocurrent. This loss of electronic charge may be compensated by various means, but the difficulty remains of reproducibly referencing the binding energies of the spectral features. Attempts to avoid such complications involve referencing the peak positions to the Fermi level of a standard such as gold or carbon in electrical contact with the sample. This procedure implicitly assumes that the Fermi level of the reference is somehow related to a property of the polymer, which (as discussed below) is generally not the case. The study of valence bands by XPS is complicated by their low cross sections for photoemission at higher (>1 keV) photon energies; in the time required to collect a valence band (VB) spectrum the sample may suffer sufficient radiation damage to affect its electronic structure. In UPS the photoelectron inelastic mean free paths are extremely short, rendering the observed spectra unduly sensitive to surface contamination and surface-localized effects,[2a] as well as to structure in the conduction bands.[3]

Among the disadvantages of UVA are the facts that the photon energies are generally not high enough to probe the entire VB, that observed spectra are complicated convolutions of the occupied and vacant densities of states, and that the absorption lengths are extremely short, necessitating very thin film (<500 Å) or solvated samples.[4] Thus, if one is primarily interested in the bulk electronic properties of a polymer, UVA is practically eliminated from consideration. There is still the possibility of performing X-ray fluorescence[5] or electron-loss[6] experiments. However, both of these techniques require bombarding the sample with electrons at rather high power density in order to collect a spectrum, which may produce severe radiation damage in a solid polymer.

SXAS avoids most of the above difficulties and provides additional information of its own. Perhaps the most definitive data supplied by SXAS are the energies of the core-level absorption edges, which yield unambiguous energy differences between each of the initial states and the particular final states accessed. Chemical-shift (oxidation state) information is also contained in core-level edge measurements. A further advantage of choosing a core level as the initial state in an absorption experiment is that it yields a truer picture of the conduction band than UVA, because the initial state has a simple line shape. Also, dipole selection rules require that only the final states with particular symmetries will be excited. For example, excitation of an s-like core level will yield the p-like partial density of unoccupied states. Absorption measurements also sample bulk properties of the polymer; thus surface perturbations are minimized. Because transmitted photons are counted with high efficiency, radiation exposure time and consequent damage are negligible. Perhaps the most appealing aspect of SXAS lies in the extended fine structure (EXAFS) above the absorption edges. The (properly treated) Fourier transform of this spectral structure yields a radial distribution function for the neighbors of the absorber that can provide morphological information even for amorphous polymeric materials. Knowledge of polymer chain topology is necessary not only for the understanding of mechanical behavior but also for use as input data for theoretical electronic-structure calculations, which can provide the necessary unification of spectroscopic data needed to understand a particular polymer system.

The application of SXAS to polymer films has been delayed for four principal reasons. First, radiation in the energy regime suitable for these studies, ca. 200–1000 eV, is available in a continuous band of sufficient intensity only at synchrotron radiation sources. Second, the available monochromators in this range usually suffer severely from poor resolution at the higher energies, higher order harmonic transmission, and carbon contamination of the optical elements, which leads both to severe attenuation of flux at the most crucial energies and to production of a scattered light background. The third problem is related in that the sensor used to detect the transmission signal must be tailored to the radiation source and the absorber studied; ideally it should have a high sensitivity over the photon energy range of interest, yet discriminate against higher order radiation transmitted by the monochromator. The final problem area involves the samples themselves. They should ideally be free-standing thin films with a mass/area ratio of 50–100 $\mu g/cm^2$ (this corresponds to a film thickness of several thousand angstroms and is the mass density that should yield a 10% transmittance signal above the carbon K edge). Also, because of the close proximity of the K edges in the light elements, EXAFS data will be difficult to collect over a sufficient energy range to allow analysis of a real-space transform (radial distribution function of the absorber) due to interference among the edges.

In this paper we show that, in spite of these difficulties, meaningful results can now be obtained from SXAS in polymers. The data reported here are presented in the spirit of an initial "survey" type of study, which we feel is particularly germane now in light of the imminent emergence of several synchrotron radiation sources throughout the world and the rapid development of experimental technology associated with synchrotron light. The present investigation of PVF_2 illustrates the entire range of information to be gained from SXAS studies of polymers. This may help workers interested in the chemistry and physics of polymers to evaluate SXAS as a viable spectroscopic tool. It also demonstrates the requirements that SXAS research places on the development of synchrotron radiation facilities.

III. Experiments

The experiments were performed on the 4° port[8] of Beam Line I at the Stanford Synchrotron Radiation Laboratory (SSRL).[9] The experimental apparatus has been described in detail elsewhere,[10,11] and will only be briefly discussed here.

The vacuum restrictions of the radiation source and the short attenuation lengths in the soft X-ray spectral regime require that the sample and detector be maintained in an ultrahigh-vacuum

(3) K. Seki, S. Hashimoto, N. Sato, Y. Haroda, K. Ishii, H. Inokuchi, and J. Kanbe, *J. Chem. Phys.*, **66**, 3644 (1977).
(4) M. T. Vala, Jr., J. Haebig, and S. A. Rice, *J. Chem. Phys.*, **43**, 886 (1965).
(5) R. E. LaVilla, *J. Chem. Phys.*, **58**, 3841 (1973).
(6) G. R. Wright and C. E. Brion, *J. Electron Spectrosc. Relat. Phenom.*, **4**, 347 (1974); J. J. Ritsko, L. J. Brillson, R. W. Bigelow, and T. J. Fabish, *J. Chem. Phys.*, **69**, 3931 (1978); J. J. Ritsko and R. W. Bigelow, *ibid.*, **69**, 4162 (1978).
(7) F. W. Lytle, D. E. Sayers, and E. A. Stern, *Phys. Rev. B*, **11**, 4825 (1975).
(8) F. C. Brown, R. Z. Bachrach, S. B. M. Hagström, N. Lien, and C. H. Pruett, "Vacuum Ultraviolet Radiation Physics", E. E. Koch, R. Haensel, and C. Kunz, Eds., Pergamon Press, Oxford, 1974, p 785.
(9) H. Winick in ref 8, p 776.
(10) J. Stöhr and D. Denley, "Workshop on X-ray Instrumentation for Synchrotron Radiation Research", H. Winick and G. Brown, Eds., Stanford Synchrotron Radiation Laboratory Report No. 78/04, p 8-181, unpublished.
(11) D. Denley, R. S. Williams, P. Perfetti, D. A. Shirley, and J. Stöhr, *Phys. Rev. B*, **19**, 1762 (1979).

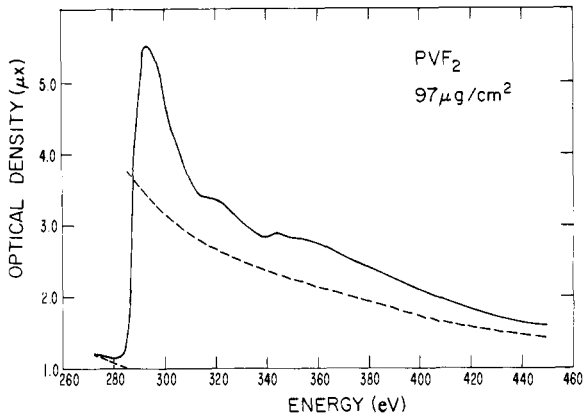

Figure 1. Absorption spectrum for PVF_2 in the vicinity of the C K edge. The dashed line is the calculated atomic absorption.

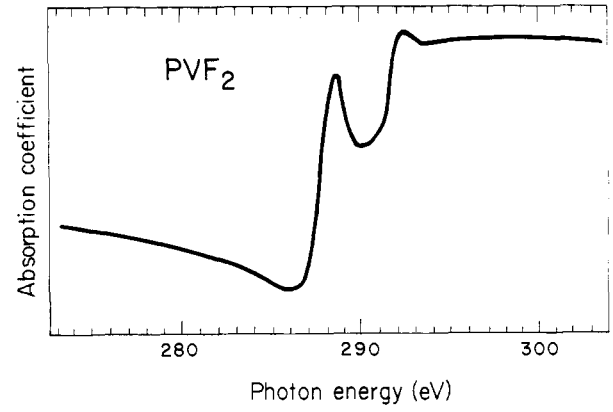

Figure 2. A higher resolution scan at the C K edge showing the compound structure at 288.6 and 292.5 eV.

environment. A beam collimator/filter, the sample holder, and the photon detector were all contained in a single chamber pumped by a 60 L s^{-1} noble ion pump and a Ti sublimation pump; the chamber pressure was $<3 \times 10^{-9}$ torr during the experiments. The beam collimator/filter was necessary to define the beam by eliminating the scattered light background and filtering out higher harmonics of the primary frequency passed by the diffraction grating at the lower energies utilized in this absorption study. A microprocessor/controller drove a motor-and-cam arrangement that allowed the absorption sample and a reference blank to intercept the beam position alternately at every monochromator setting, thus allowing the immediate computation of a ln (I/I_0) signal. Radiation detection was achieved by impinging the transmitted radiation on a solid absorber film, such as ZnS or Au, and collecting the signal as the total photoyield measured by a channeltron electron multiplier. This arrangement allowed stable amplification of the signal and enabled us to match the properties of the detector to both the absorber and the region of the monochromator band-pass utilized.[10]

The PVF_2 used was obtained from the Pennwalt Corp. as a commercial powdered resin (brand name Kynar). No further purification of the resin was attempted. Thin films were grown by dipping clean glass microscope slides into a 2% (by weight) solution of PVF_2 in reagent-grade tetrahydrofuran. After drying, each film was floated off its slide by dipping it into a water bath. Films so produced were then dried to a constant weight and measured to determine their areas. A small (7×5 mm) sample was then cut from each film and mounted on a sample holder. The films were transparent, pinhole-free, and self-supporting. The above sample-preparation technique is expected to yield semicrystalline PVF_2 films composed primarily of α-phase[2] (or phase II)[12,13] crystallites, which have a reported density of 1.93 g/cm^3. Thus, the 97 μg/cm^2 film used in this study was $\sim$5000 Å thick.

IV. Results

A. The Carbon K-Edge Spectral Region. Figure 1 shows an uncorrected SXAS spectrum of PVF_2 collected over the energy range 270–450 eV. The important features in this spectrum are the sharp peak at the onset of absorption and the structure in the spectrum near 343 eV, which is due to attenuation of second-order light by fluorine K-edge absorption. Second-order light was found to comprise ca. 3.5 and 2.5% of the total radiation intensity at 300 and 400 eV, respectively, as measured through a Ti filter by a ZnS photocathode detector. Thus, even using a filter to attenuate radiation above 455 eV (the Ti $L_{2,3}$ edge) and a detector with a decreasing photoyield with energy, the carbon K-edge region absorption spectrum suffers from high-order interference; therefore, we did not attempt to Fourier transform the carbon K-edge data.

The absorption spectrum in Figure 1 is comprised of a large, broad peak which joins smoothly to the carbon K-edge continuum structure. The amplitude of the peak structure is actually suppressed owing to the second-harmonic interference; allowing a correction for this effect yields an "adjusted" optical density of 5.5 for the peak maximum. Also plotted in Figure 1 is the "theoretical" optical density of a 97 μg/cm^2 film of PVF_2, computed from the atomic absorption cross sections of C and F compiled by Veigele.[14] The agreement between this prediction and the measured values is excellent below the C K edge (where the ratio of second-harmonic radiation to primary is very small) and at the higher photon energies shown, which lends credence to the ability of the present measurements to obtain accurate quantitative determinations. However, comparison of the peak height in the present measurements to a similar peak preceding the C K edge in the reported absorption spectra of gaseous fluorinated methanes[15] would yield an optical density of 68.1 (for a carbon atom cross section of 14 Mb) for our PVF_2 sample, over an order of magnitude higher than the corrected value of 5.5 stated above. The discrepancy is attributed to an error in the cross-section determination in the fluoromethanes, which was much higher than predicted by Veigele.[14]

A more detailed plot of the absorption onset region is given in Figure 2. The large peak preceding the absorption edge is actually a doublet, at 288.6 and 292.5 eV. The 3.9-eV separation between these two peaks corresponds quite well to the energy difference between the main peaks observed for gaseous CH_4 and CH_2F_2 at 288 and 292 eV, respectively. Thus, they most likely arise due to excitations from the 1s level to the (localized) lowest lying molecular orbitals of the correct symmetry for the two chemically inequivalent carbon species in PVF_2. The observed peaks may be the initial and most intense members of a molecular Rydberg series (as expected from atomic theory),[16] leading up to the polymer's ionization potential.

The carbon K-edge absorption data may also be compared to XPS studies of PVF_2.[17,18] The splitting observed in the discrete absorption doublet agrees fairly well with the chemical shift of 4.5 eV observed between the C(1s) signals in the XPS spectrum.[17,18] This is consistent with the expectation that the discrete doublet is due to excitations from the two chemically inequivalent carbons in PVF_2 to the lowest unoccupied molecular states. However, the splittings obtained in photoemission and in absorption should not necessarily be equal. Studies by Duke et al.[19]

(12) J. B. Lando, H. G. Olf, and A. Peterlin, *J. Polym. Sci., Part A-1*, **4**, 941 (1966).
(13) R. Hasegawa, Y. Takahashi, Y. Chatani, and H. Tadokoro, *Polym. J.*, **3**, 600 (1972).
(14) W. J. Veigele, *At. Data*, **5**, 51 (1973).
(15) R. Z. Bachrach, F. C. Brown, A. Bianconi, and H. Petersen, Stanford Synchrotron Radiation Laboratory Report No. 77/16, unpublished; *Chem. Phys. Lett.*, **54**, 425 (1978).
(16) U. Fano and J. W. Cooper, *Rev. Mod. Phys.*, **40**, 441 (1968).
(17) D. T. Clark, W. J. Feast, D. Kilcast, and W. K. R. Musgrave, *J. Polym. Sci., Polym. Chem. Ed.*, **11**, 389 (1973).
(18) J. J. Pireaux, J. Riga, R. Caudano, J. J. Verbist, J. M. Andre, J. Delhalle, and S. Delhalle, *J. Electron Spectrosc. Relat. Phenom.*, **5**, 531 (1974); J. Delhalle, S. Delhalle, J. M. Andre, J. J. Pireaux, J. Riga, R. Caudano, and J. J. Verbist, *ibid.*, **12**, 293 (1977).

have shown that electronic transitions in polymers and molecular solids are more highly localized than normal band theory allows. Thus, the allowed final states for electronic transitions originating on chemically inequivalent sites may not fall at the same energy, because constituents such as fluorine can cause chemical shifts in the energies of the local "conduction" states, just as they do in the core levels (although these shifts should be smaller than core-level shifts owing to the spatially more diffuse nature of the levels involved). Indeed, the absorption doublet structure is split by 0.6 eV less than the chemical shift of the C(1s) photoemission peaks. The explanation for this significant difference may be phrased in several different manners, but the essential feature is that the final states in an absorption experiment are also subject to chemical shifts that are observable due to their highly localized nature.

Another interesting comparison with the XPS data lies in the absolute numbers presented for the photoemission C(1s) binding energies. Clark et al.[17] reported values of 286.1 ± 0.1 and 290.6 ± 0.1 eV for the 1s binding energies of the chemically inequivalent carbons in PVF_2, referenced to a binding energy of 83.8 eV relative to the Fermi energy for the Au $4f_{7/2}$ line. The absolute energy calibration of the PVF_2 spectra was achieved by using the C(1s) signal from the background vacuum contaminants as a standard. Pireaux et al.[18] have determined binding energies of 286.4 ± 0.1 and 290.9 ± 0.1 eV by referencing the PVF_2 spectra to the C(1s) line of polyethylene, which had previously been determined to be 284.6 eV[20] with respect to the gold Fermi level for a gold $4f_{7/2}$ binding energy of 83.8 eV. Both of the above determinations were therefore supposedly given with respect to the Fermi level of Au. However, comparison of photoemission data to absorption results is complicated by attempts to reference the XPS results to a Fermi level, even if charging effects have been properly handled. This important and general problem is discussed below.

Referencing XPS spectra of a wide-band-gap molecular solid or polymer with respect to the Fermi level of a metal in electrical contact with the insulating sample does not yield binding energies that are intrinsic properties of the unperturbed sample. Rather, these binding energies are specific to the particular insulator/metal interface. Contact charge exchange experiments[21,22] have shown that the Fermi level of a metal at a polymer–metal interface may fall anywhere within the band gap, above the "conduction band" minimum, or even below the valence-band maximum of the unperturbed polymer. Upon electrical contact with a polymer surface, the Fermi level of a metal does not equilibrate with the "Fermi level" of the insulator. The ionic states formed by the initial charge transfer between polymer and metal do not delocalize throughout the polymer sample. Thus, a charged layer builds up at the polymer surface until the electrostatic potential due to the charged surface is effectively equal in magnitude and opposite in sign to the chemical potential difference between the polymer and metal.

Thus, XPS binding energies of solid insulators in which ionic states are highly localized can vary with the metal standard used as a reference. A more meaningful reference for XPS spectra of insulators is the VB maximum energy, as determined by the onset of photoemission from the VB of the sample. From ref 18 this value lies at 5.8 ± 0.1 eV binding energy relative to the gold Fermi energy. The binding energies of the C(1s) signals with respect to the VB maximum are thus 280.6 ± 0.2 and 285.1 ± 0.2 eV.

Figure 3 shows a one-electron energy diagram for photoemission and absorption in PVF_2, referenced with respect to the VB maximum. The value of the energy gap of PVF_2 has been estimated at 14.1 eV,[18] which would appear to be too large in view of Figure 3. Duke[2a] has shown that predictions of such energy-level splittings in polymers that do not take account of relaxation effects

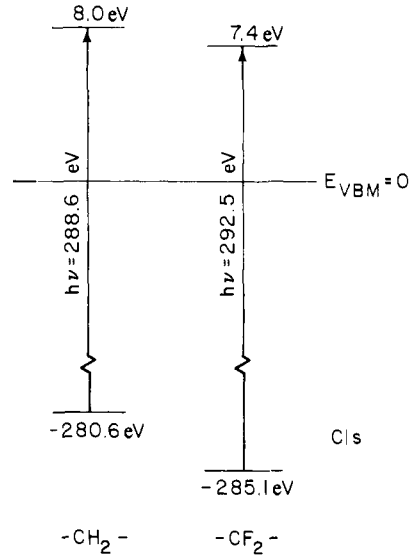

Figure 3. A one-electron energy-level diagram showing the effects of absorption at the inequivalent carbon sites. Final states may or may not lie in a forbidden gap below the onset of conduction bands, because of excitonic binding.

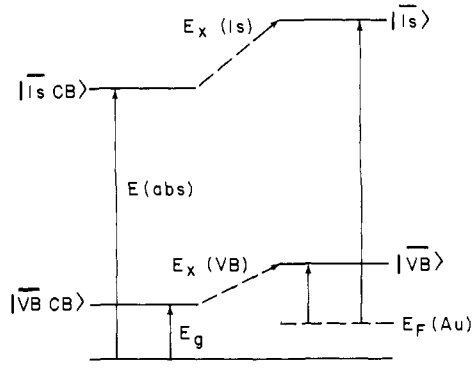

Figure 4. Energy-level diagram of the PVF_2 system, incorporating the data quoted in text. Here bars denote hole states, and the bottom line is the ground state. Absorption is shown on the left and photoemission on the right. In the latter the gold Fermi level is used as reference because photoelectron energies are usually referenced to a Fermi energy.

(many-electron effects) are generally too large. However, a relatively small band gap of 7.8 eV, which would be inferred from a naive interpretation of the absorption from the C(1s) levels of PVF_2, is almost certainly too small. Excitation of a 1s electron at threshold probably yields a localized excitonic state in which the excited molecular orbital is stabilized by the attractive force of the core hole. The one-electron picture implicit in Figure 3 is actually inadequate for describing this system, as is often the case in solid-state problems. For example, the final levels above E_{VBM} are not states to which valence electrons can be raised. The reason is that the one-electron diagram is not an energy-level diagram, but is only an approximate representation of the true energy-level structure of the system, presented *upside down*. This point was made earlier in explaining many-body excitonic effects on core-level binding energies in solids.[23]

In Figure 4 a real energy-level diagram is shown which incorporates the numerical results given above. In drawing this diagram we have used the Fermi energy of gold as a reference for the photoemission data. With a diagram of this type it is easy to explain how the absorption energy can fall several electron volts below the threshold for photoemission from the same core level. More subtly, this diagram helps us understand why the *difference* between core- and valence-electron absorption energies can exceed the difference between their binding energies. Physically, the

(19) C. B. Duke, T. J. Fabish, and A. Paton, *Chem. Phys. Lett.*, **49**, 133 (1977).
(20) J. Delhalle, J. M. Andre, S. Delhalle, J. J. Pireaux, R. Caudano, and J. J. Verbist, *J. Chem. Phys.*, **60**, 595 (1974).
(21) C. B. Duke and T. J. Fabish, *Phys. Rev. Lett.*, **37**, 1075 (1976).
(22) T. J. Fabish and C. B. Duke, *J. Appl. Phys.*, **48**, 4256 (1977).
(23) L. Ley, F. R. McFeely, S. P. Kowalczky, J. G. Jenkin, and D. A. Shirley, *Phys. Rev. B*, **11**, 600 (1975).

"excitonic" binding of an excited electron to a localized 1s hole, $E_X(1s)$, is expected to be stronger than that to a more diffuse hole in the valence band, $E_X(VB)$. This is a well-known phenomenon in molecular electron spectroscopy. From energy conservation and Figure 4 we find

$$E(\text{abs}) + E_X(1s) - E_B^F(1s) + E_B^F(VB) - E_X(VB) - E_g = 0$$

$$E_X(1s) - E_X(VB) = \Delta E_B(1s) - E_{abs} + E_g$$

$$\Delta E_X(1s) = E_g - 8.0 \text{ eV}$$

or

$$\Delta E_X(1s) = E_g - 7.4 \text{ eV}$$

depending upon whether the carbon 1s parameters for the carbon in CH_2 or CF_2 are used. Here, $\Delta E_B(1s) = E_B^F(1s) - E_B^F(VB)$ is the binding energy of the C(1s) electron referred to the valence-band "maximun", i.e., the least bound valence electrons, and $\Delta E_X(1s)$ is the *additional* excitonic binding energy of the excitonic state in the presence of a 1s hole, over that in the presence of a hole in the valence band, i.e., $\Delta E_X(1s) = E_X(1s) - E_X(VB)$. It is only possible to determine the excitonic binding energy *difference* because the VB and 1s binding energies are known only relative to a "floating" reference energy—the Fermi level of gold. To estimate the gap energy E_g we need only make a reasonable estimate of $\Delta E_X(1s)$. If the excited electrons and holes were completely delocalized, $\Delta E_X(1s)$ would be zero, and E_g would be 7.4 or 8.0 eV. The other extreme limit—that of a completely localized excitation, made up of an electron–hole point on the same carbon atom—is probably much closer to the truth. To estimate $\Delta E_X(1s)$ in this limit we invoke a simple localized model that has had some success in predicting excitonic energies in the past in systems ranging from metals[23] to Auger satellite states.[24] An atomic potential model is used, and atomic integrals are employed to estimate pairwise interaction energies. We consider the two separation processes

$$(\overline{VB}\ CB) \rightarrow (\overline{VB}) + e^- \qquad E_X(VB)$$

$$(\overline{1s}\ CB) \rightarrow (\overline{1s}) + e^- \qquad E_X(1s)$$

in which an electron is removed from the conduction band CB in the presence of either a valence-band hole or a 1s hole. The energies of the two processes are the excitonic binding energies, $E_X(VB)$ and $E_X(1s)$, respectively. The difference in these energies is approximately the difference between the Coulombic interaction of the localized CB electron with a VB electron and with a 1s hole. In the atomic limit this difference is given to first approximation by[23,24]

$$\Delta E_X(1s) \simeq F^\circ(1s,CB) - F^\circ(VB,CB)$$

Of course the atomic-orbital composition of the CB state (and the VB state) is a priori unknown. In the extreme limit that both are assumed to be 2p orbitals, we have

$$\Delta E_X(1s) \simeq F^\circ(1s,2p) - F^\circ(2p,2p) = 6.6 \text{ eV}$$

where Mann's integrals[25] have been employed to estimate a numerical value. This result is to be regarded as an extreme upper limit. The limits on E_g are therefore roughly given by $8 \text{ eV} \leq E_g \leq 14$ eV. This is a very broad range for E_g, but we note that, if the position of $E_F(Au)$ were known absolutely, it would be possible to deduce $E_X(1s)$ from the data, rather than only $\Delta E_X(1s)$, and thereby to gain more understanding of plausible values of E_g. The main value of this analysis is to show how absorption and XPS data can be combined into a meaningful energy-level diagram.

An estimate of the excitonic binding $E_X(1s)$ for localized states can be obtained by comparison of the absorption edge energies

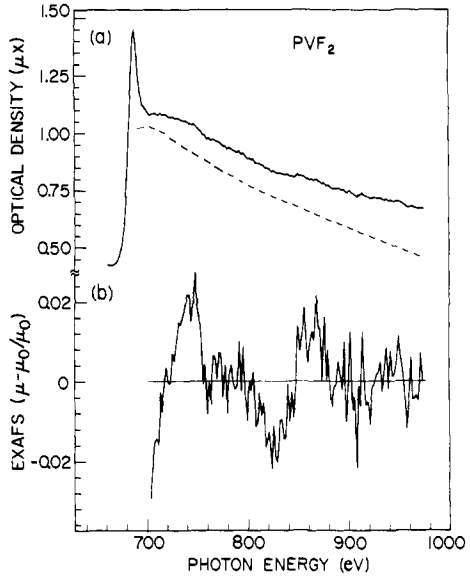

Figure 5. (a) Absorption spectrum of PVF_2 above the F K edge. The dashed line is the calculated atomic absorption curve. (b) The residual EXAFS spectrum after the subtraction of a smooth background.

and core-level binding energies for C(1s) electrons in CH_2F_2 and CH_4. Noting that carbon and hydrogen are of comparable electronegativity, the central carbons in the (C)–CH_2–(C) and (C)–CF_2–(C) groups in PVF_2 can be simulated by the gas-phase model compounds in H–CH_2–H and H–CF_2–H, respectively. Because the reference level in gas-phase photoemission is unambiguously the ground state, we have (cf. Figure 4)

$$E_B(1s) = E(\text{abs}) + E_X(1s)$$

From the numerical values[26,27]

$$E_B(\text{C1s, } CH_4) = 290.8 \text{ eV}$$

$$E_B(\text{C1s, } CH_2F_2) = 296.4 \text{ eV}$$

and for the most intense peaks[28]

$$E(\text{abs, } CH_4) = 288.1 \text{ eV}$$

$$E(\text{abs, } CH_2F_2) = 292.9 \text{ eV}$$

Thus for these molecules

$$E_X(\text{1s, } CH_4) = 2.7 \text{ eV}$$

$$E_X(\text{1s, } CH_2F_2) = 3.5 \text{ eV}$$

These values of E_X are about half the size of those estimated above for $\Delta E_X(1s)$. Taking these latter values to be upper limits for PVF_2 exciton energies, we would have

$$E_g(CH_2) \sim 8.0 + 2.7 = 10.7 \text{ eV}$$

$$E_g(CF_2) \sim 7.4 + 3.5 = 10.9 \text{ eV}$$

Consequently, our best estimate for E_g is ~10–11 eV.

B. The Fluorine K-Edge Spectral Region. The PVF_2 absorption spectrum in the energy range 780–1000 eV is shown in Figure 5 along with the absorption curve above the fluorine K edge predicted by using atomic absorption cross sections.[18] The spectrum is remarkably similar in general appearance to the fluorine K-edge spectra of the fluorinated methanes obtained by LaVilla.[5] Approximating the cross section of fluorine at the maximum absorption as 0.95 Mb (half the maximum cross sections

(24) D. A. Shirley, *Phys. Rev. A*, **9**, 1549 (1973).
(25) J. B. Mann, Los Alamos Scientific Laboratory Report No. LASL-3690, 1967 (unpublished).
(26) T. D. Thomas, *J. Am. Chem. Soc.*, **92**, 4184 (1970).
(27) D. W. Davis, D. A. Shirley, and T. D. Thomas, *J. Chem. Phys.*, **56**, 671 (1972).
(28) F. C. Brown, R. Z. Bachrach, and A. Bianconi, *Chem. Phys. Lett.*, **54**, 425 (1978).

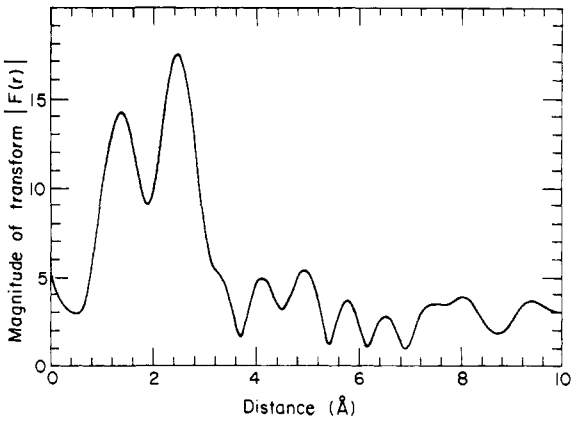

Figure 6. Fourier transform of the EXAFS data after inclusion of a compensating factor for the phase shift. The second large peak is due to a number of higher neighbor shells (see Table I).

for CH_2F_2) yields an optical density value of $\mu x = 2.0$ for the peak height in Figure 5a. The observed value of 1.45 for the optical density is in good agreement with this prediction from gas-phase results.

The main feature of interest in this spectrum is the modulation above the fluorine K edge, which is shown in an expanded plot in Figure 4b. In principle, such EXAFS oscillations should yield accurate interatomic distances in the polymer chain. These distances are extremely important in determining the space group of a crystal and the unit-cell dimensions, then finding the best cell and chain structures that are compatible with the X-ray data, using tabulated collections of bond lengths.[29] Clearly, a superior structure may be determined if one knows the actual bond lengths of the material studied.

In general, a radial distribution function can be deduced from the EXAFS data if the effects of phase shifts in the electron wave due to the atomic potentials are compensated. Figure 6 shows a plot of the radial distribution function

$$R(r) = |F(r)| = \left|\int dk e^{-i2kr} \frac{e^{i\phi(k)}}{A(k)} k\chi(k)\right| \quad (1)$$

where χ is the extended absorption fine structure signal, $A(k)$ is the amplitude function for backscattering taken from tabulated values,[30] and ϕ is the total phase shift experienced by an electron in traveling to a neighboring atom from the absorbing site and back.[31] The wave vector of the electron is given by

$$k = 0.5123(h\nu - E_0 + E_i)^{1/2}\ \text{Å}^{-1} \quad (2)$$

with energies expressed in eV; E_0 is the energy at the onset of absorption. The work of Lee and Beni[32] suggests that the inner potential, E_i, should be adjusted until the peaks in $R(r)$ and Im $\mathcal{F}(r)$ coincide. We note that this rule is valid only if the separation between neighbor shell distances sufficiently exceeds the peak half-width (which results from the finite data range). In fact, a calculation shows that, for an experimental data window extending from k_1 and k_2, the radial distribution function from a doublet of close neighbor shells at distances r_1 and r_2 will result in an unresolved peak if $r_2 - r_1 \approx [\pi(k_2 - k_1)]^{-1}$. As we describe below, the rule of Lee and Beni breaks down in our PVF_2 measurements for all shells beyond the first. Accordingly, we chose $E_i = 5$ eV, to bring the first peak in $R(r)$ into line with the corresponding peak in Im $\mathcal{F}(r)$.

The first peak corresponds to the F–C bond distance, which was assumed in previous X-ray work[13] to be 1.34 Å. The value found in the present work is 1.38 ± 0.02 Å. This value was obtained by using as the fluorine-to-carbon backscatterer-phase function[31]

$$\phi = -6.050 - 1.0882k + 0.0323k^2 \quad (3)$$

where k is given in units of $Å^{-1}$. The second peak at 2.45 ± 0.08 Å consists of contributions from several further neighbor shells. The model of Hasegawa et al.[13] yields nine higher neighbor shells in the polymer chain at distances below 3 Å (at greater distances there will also be interchain neighbors). Because the overall amplitude dependence of the EXAFS signal[32] goes roughly as

$$Q_i = N_i/R_i^2$$

certain deductions can be made about the nearby structure by comparing a mean of the secondary and tertiary neighbors (see Table I) weighted by Q_i to the observed peak position. There may be a decrease in the long-range order for a significant fraction of the PVF_2 sample beyond the secondary shell. In the tertiary shell this could occur through a decrease in the effective Debye–Waller factor, $e^{-2\sigma_i^2k^2}$, an increase in $\sigma_{\text{tertiary}}^2$, or the existence of disorder in the dihedral angle between tertiary neighbors. The expected results of such disorder would be to "wash out" the high end of the secondary–tertiary distribution, thereby shifting the peak to lower values compared to the "ideal" mean, which was computed[33] to be 2.42 Å. That this is not at all the case implies that strong ordering exists in PVF_2 through the tertiary neighbor shell. All of the remaining peaks are much weaker and too dependent in their positions upon the details of the background subtraction to make a reliable interpretation.

The presence of disorder in PVF_2 is quite evident in comparing its X-ray diffraction patterns to those of any well-ordered crystal. However, there is clear evidence in the present measurements that the estimate of the thermal disorder ($\sigma^2 = 5$ Å^2 by Hasegawa et al.)[13] is much too great. In fact, a fit of the data with the modified distances in Table I yields a least-squares fit for $\sigma^2 \approx 0.07$ Å^2. A more accurate value could be obtained with a more accurate structure.

Table I. PVF_2 Neighbor Frequencies from the Model of Hasegawa et al.

neighbors	bond connection	distance,[a] Å	number, N_i, per F absorber[b]	quality factor[c]
F to C	direct	1.34 (1.38)	1	1.00
F to F	secondary[d]	2.10 (2.16)	1	0.41
F to C	secondary	2.24 (2.27)	0.5	0.18
F to C	secondary	2.35 (2.38)	0.5	0.16
F to C	secondary	2.36 (2.39)	0.5	0.16
F to C	secondary	2.39 (2.42)	0.5	0.16
F to F	tertiary[e]	2.70 (2.70)	0.5	0.13
F to C	tertiary	2.76 (2.77)	0.5	0.066
F to C	tertiary	2.85 (2.87)	0.5	0.064
F to C	tertiary	2.95 (2.99)	0.5	0.057

[a] Parenthetical values are the values that result from assuming an increase of the F–C bond length from 1.34 to 1.38 Å. [b] There are two inequivalent F absorber sites. [c] Quality factor $Q_i = N_i(1.38/R_i)^2$. [d] That is, two bonds "distant" from each other. [e] Three bonds "distant" from each other.

V. Conclusion

In summary, it is clear that absorption measurements in the soft X-ray region can yield useful information. Once the stringent requirements on vacuum and sample thickness are met, the measurements can be made rapidly. We have found a differential carbon K-edge chemical shift between CH_2 and CF_2 sites in good agreement with XPS measurements. With the value of the PVF_2 band gap of ~10–11 eV, the onset of absorption corresponds to transitions to bound states several electron volts below the con-

(29) "International Tables for X-ray Crystallography", Vol. I–III, Kynoch Press, Birmingham, England, 1962.
(30) B.-K. Teo, P. A. Lee, A. L. Simmons, P. Eisenberger, and B. M. Kincaid, *J. Am. Chem. Soc.*, **99**, 3854 (1977).
(31) P. A. Lee, B.-K. Teo, and A. L. Simons, *J. Am. Chem. Soc.*, **99**, 3856 (1977); B.-K. Teo and P. A. Lee, private communication.
(32) P. A. Lee and G. Beni, *Phys. Rev. B*, **15**, 2862 (1978).
(33) Approximately 0.04 Å must be added to the two F–F distances to account for the small differences of the F to F phase from the F to C phase function.

duction band edge for the carbon sites. In addition to the electronic structure information, we were able to determine the F-C bond length to be 1.38 Å and we also found indications that structural ordering holds strongly through the tertiary neighbors to fluorine.

Acknowledgments. This work was performed at the Stanford Synchrotron Radiation Laboratory, which is supported by the NSF Grant 77-27489, in cooperation with the Stanford Linear Accelerator Center and was done with support from the Division of Chemical Sciences, Office of Basic Energy Sciences, U.S. Department of Energy, under Contract W-7405-Eng-48. The authors wish to thank Peter Young, Gustav Apai, and Paul Wehner for their contributions to the early stages of this work, Wini Heppler for making the thin films used in this study, and Joseph Katz and Richard Strudwick for designing and building the electronics that made the experiment possible.

Rotational Motions of Side Chains of Poly-L-lysine

Richard J. Wittebort, Attila Szabo, and Frank R. N. Gurd*

Contribution from the Department of Chemistry, Indiana University, Bloomington, Indiana 47405. *Received March 10, 1980*

Abstract: The ^{13}C NMR relaxation times and nuclear Overhauser enhancements have been measured for the protonated carbons of poly-L-lysine at 15.1 and 67.9 MHz. To characterize the structure of the polylysine we have examined both the CD and ^{13}C NMR spectra at 3 and 28 °C at pH values between 10 and 11 in the neighborhood of the helix-coil transition. At 3 and 28 °C for pH values above the completion of the random coil-helix transition the peptide readily aggregates at the concentrations used. Consequently, to avoid the aggregation, we have studied the NMR relaxation under the conditions 3 °C and pH 10.7, where the poly-L-lysine does not have a rigidly structured α-helical backbone. The relaxation data are interpreted in terms of a recently developed theoretical formalism. The simplest model for the molecular motions consistent with the frequency-dependent NMR data assumes that backbone carbons, C^{α}, are characterized by a distribution of correlation times, or diffusion constants as used here, and the side-chain carbons, C^{β}, C^{γ}, C^{δ}, and C^{ϵ}, undergo independent axial motions with *restricted* angular amplitudes.

High-resolution nuclear magnetic relaxation studies can, at least in principle, give detailed information about rotational dynamics of molecules in solution. This is because the relatively low, i.e., radio, absorption frequency of NMR experiments conveniently coincides with the characteristic frequencies of molecular rotational motions in condensed phases. In this study we apply a recently developed theoretical formalism[1,2] to extract detailed motional information from the ^{13}C longitudinal relaxation times and nuclear Overhauser enhancements of the protonated carbons in poly-L-lysine.

A similar study of poly(*n*-alkyl methacrylates) has been reported by Levy et al.[3] These authors attempted to describe their relaxation data in terms of a generalization of a model proposed originally by Wallach.[4] The side-chain *n*-alkyl carbons are assumed to be undergoing consecutive independent and free axial diffusion-like motions about the C-C bonds. The side-chain motion is superimposed on isotropic backbone motion which, as suggested by Schaefer,[5] is characterized by a distribution of correlation times or rotational diffusion constants. These authors found that the frequency-dependent relaxation data of the side-chain carbons is not consistent with this description.

One expects that the assumption of free axial motions about the side-chain C-C bonds is unrealistic in that the allowed conformational space is too large. The Wallach model has recently been generalized by Wittebort and Szabo[1] to incorporate excluded volume effects by restricting the *amplitude* of internal rotations and, independently, by London and Avitabile[2] for the case of a single internal rotation. In this study we further extend the model to allow the α carbon to possess a distribution of rotational correlation times. In order to make this model computationally feasible, a distribution function for the backbone diffusion constants was chosen such that the required averages of the spectral density functions could be performed analytically rather than numerically as has been done previously for the Wallach model.[3]

Materials and Methods

The polylysine used in this study was prepared by Miles-Yeda Ltd. and obtained from Miles Laboratories, Elkhart, Ind. The material, Code 71-120, Lot 250, and molecular weight 27 000, had a degree of polymerization of 129.

Polylysine samples in 0.1 M NaF were prepared by dissolving 660 mg of the HBr salt in 12 mL of deionized and distilled H_2O. The solution was titrated to pH 10.6 by the addition of redistilled HCl at 3 °C, and then dialyzed overnight against H_2O. Subsequently, the volume was decreased to the original 12 mL and sufficient NaF was added to be 0.1 M in this salt. The pH was adjusted to the desired value at 25 or 3 °C prior to the NMR experiment.

^{13}C NMR spectra were obtained on home-built spectrometers operating at either 15.01 or 67.9 MHz. The 90° H_1 pulse widths on the two spectrometers were typically 37 μs (15.1 MHz spectrometer) or 18.5 μs (67.9 MHz spectrometer) and were redetermined prior to each relaxation study. Relaxation studies were done by using the inversion recovery method, i.e., 180°-τ-90° pulse sequences. T_1 values were determined from the inversion recovery experiments by fitting the intensities, $I(\tau)$, of each NMR line to the function $I(\tau) = A + Be^{-T_1/\tau}$, using a nonlinear least-squares fitting program, BMDX85.[6,7]

Nuclear Overhauser enhancements, NOE's, were measured at 67.9 MHz, using the gated decoupling method with 100-Hz square-wave modulation and a recycle time of 4.0 s. Error analysis of the NOE values was carried out by calculating the standard deviation, σ, in the integrated intensities, I_G, of the protonated carbon resonances in the spectrum obtained with gated decoupling. Since all resonances in this spectrum should have the same intensity, σ is a measure of the uncertainty in these values. The uncertainties for the NOE values were calculated from the relation $NOE_{\pm} = (I_{cw} \pm \sigma)/(I_G \mp \sigma)$ where NOE_+ and NOE_- are taken

(1) Wittebort, R. J.; Szabo, A. *J. Chem. Phys.* **1978**, *69*, 1722.
(2) London, R. E.; Avitabile, J. *J. Am. Chem. Soc.* **1978**, *100*, 7159.
(3) Levy, G. C.; Axelson, D. E.; Schwartz, R.; Hockmann, J. *J. Am. Chem. Soc.* **1978**, *100*, 410.
(4) Wallach, D. *J. Chem. Phys.* **1967**, *47*, 5258.
(5) Schaefer, J. A. *Macromolecules* **1973**, *6*, 882.
(6) Kowalewski, J.; Levy, G. C.; Johnson, L. F.; Palmer, L. *J. Magn. Reson.* **1977**, *26*, 533.
(7) Dixon, W. J., Ed., 1965, BMD Biomedical Computer Programs, University of California Press: Los Angeles, BMDX85, April, 1971, revision, developed at the Health Sciences Computing Facility, UCLA, sponsored by NIH Special Research Resources Grant RR-3.

0002-7863/80/1502-5723$01.00/0 © 1980 American Chemical Society